Chimica Techno Acta
published by Ural Federal University
eISSN 2411-1414
chimicatechnoacta.ru

ARTICLE
2024, vol. 11(4), No. 202411403
DOI: 10.15826/chimtech.2024.11.4.03

The novel Zn-doped hexagonal perovskite $Ba_7In_6Al_2O_{19}$: electrical conductivity and hydration

Irina Animitsa, Daniil Korona, Arina Bushueva,
Roman Andreev, Sergey Nokhrin

Institute of Natural Sciences, Ural Federal University, Ekaterinburg 620009, Russia
* Corresponding author: irina.animitsa@urfu.ru

This paper belongs to a Regular Issue.

Abstract

The novel phase $Ba_7In_{5.9}Zn_{0.1}Al_2O_{18.95}$ with hexagonal perovskite structure was obtained by solid-state technique. The substitution of In^{3+} by the Zn^{2+} leads to the expansion of the lattice parameters and cell volume. It was established that the investigated sample is capable of water incorporation from the gas phase; the degree of hydration reaches 1.42 mol H_2O, which is significantly higher than that for the undoped phase (0.41 mol H_2O). This is a result of the expansion of the hexagonal layer that facilitates the placement of OH^--groups. The oxide-ion and proton conductivities for the doped $Ba_7In_{5.9}Zn_{0.1}Al_2O_{18.95}$ sample were higher than those for the undoped composition, $Ba_7In_6Al_2O_{19}$, by 0.50 and 0.75 orders of magnitude (500 °C), respectively. The new phase $Ba_7In_{5.9}Zn_{0.1}Al_2O_{18.95}$ demonstrates the predominant protonic conductivity at $T \le 500$ °C and $pH_2O = 1.93 \cdot 10^{-2}$ atm.

Keywords

hexagonal perovskite
proton conductivity
hydration
transport numbers

Received: 24.0824
Revised: 09.09.24
Accepted: 11.09.24
Available online: 30.09.24

Key findings

- A novel hexagonal perovskite $Ba_7In_{5.9}Zn_{0.1}Al_2O_{18.95}$ has been synthesized.
- $Ba_7In_{5.9}Zn_{0.1}Al_2O_{18.95}$ is capable of dissociative water molecule incorporation.
- $Ba_7In_{5.9}Zn_{0.1}Al_2O_{18.95}$ is able to exhibit proton conductivity.
- $Ba_7In_{5.9}Zn_{0.1}Al_2O_{18.95}$ demonstrates predominant proton transport at $T \le 500$ °C in wet air.
- The Zn^{2+}-doping of $Ba_7In_6Al_2O_{19}$ increases the oxide-ion and proton conductivities.

1. Introduction

High-temperature proton conductors, first described by H. Iwahara more than 40 years ago [1, 2], are still being intensively studied, since they are promising electrolytes for solid oxide fuel cells, which are highly efficient, environmentally friendly and economically attractive electrochemical devices. At present, high values of proton conductivity have been achieved for acceptor-doped perovskites – barium cerates and zirconates $Ba(Ce,Zr)O_3$ [3–5], but their chemical stability is unsatisfactory due to degradation in atmospheres containing CO_2 [6–16]. Primarily, the creation of new proton-conducting complex oxides occurs both by modifying the composition of known compounds and by complicating the structure [17–19].

In the 20s, high-temperature proton transport was also discovered in a more complex structural type – hexagonal perovskite-like compounds built according to the block principle from fragments of various structural types [20–23]. For example, the compounds $Ba_5M_2Al_2ZrO_{13}$ (M = Gd–Lu, Y, Sc, In) [24] and $Ba_5M_2Al_2SnO_{13}$ (Gd, Dy, Ho, Y, Tm, Yb) [25] can be represented as an intergrowth of a perovskite block $Ba(Zr,Sn)O_3$ and two oxygen-deficient blocks $Ba_2M^{3+}AlO_5$. Among them, the most conductive are the Er-containing phases $Ba_5Er_2Al_2ZrO_{13}$ and $Ba_5Er_2Al_2SnO_{13}$, although the relationship between the nature of the cations and the magnitude of proton conductivity is not yet clear. Owing to the presence of blocks containing unoccupied oxygen positions, such phases are capable of incorporating water without doping. For example, zirconates can incorporate 0.23 mol H_2O for $Ba_5Er_2Al_2ZrO_{13}$ and 0.30 mol H_2O for $Ba_5In_2Al_2ZrO_{13}$ [26]. Stannates $Ba_5M_2Al_2SnO_{13}$ (Gd, Dy, Ho, Y, Tm, and Yb) exhibited water uptakes within $0.48 \le x \le 1.00$ at 100 °C depending on the nature of the rare earth metals [25]. Among these oxides, the phase that exhibited the greatest water uptake of 1 mol H_2O was $Ba_5Er_2Al_2SnO_{13}$ [25]. It is not yet possible to establish any specific relationships between nature of the elements in the compound and water uptake, as the experimental data are still very limited. However, since it has been clearly shown that the incorporation of water molecules occurs in the oxygen-deficient layer, its size will be an important characteristic of hydration.

Investigations of the influence of doping on transport properties have been performed only for $Ba_5In_2Al_2ZrO_{13}$ [26–29], and it has been shown that not only acceptor doping but also isovalent substitution can improve the ionic (O^{2-}, H^+) conductivity. That is, the role of the geometric factor in ion transport is obvious.

The other composition with a hexagonal perovskite structure $Ba_7Nb_4MoO_{20}$ is formed by a combination of perovskite and palmierite-like layers [19]. The compound is composed of isolated tetrahedral units that have a particular topology that allows water incorporation and fast ionic transport. The phase can incorporate 0.80 mol H_2O, and this value is close to the theoretical solubility limit of one water molecule per formula unit, corresponding to one oxygen vacancy per formula unit of $Ba_7Nb_4MoO_{20}$. A strategy to increase the oxide-ion conductivity of this phase involves the introduction of an element with a higher oxidation state (donor doping), such as molybdenum or tungsten, into the niobium positions. The positive effect is explained by filling interstitial oxygen sites. However, the effect of such substitution on proton transport is ambiguous. For example, proton conduction in $Ba_7Nb_4MoO_{20}$ is critically reduced when niobium is replaced by tungsten (+6) or chromium (+6) [30, 31].

A more complex example of intergrowth structure is $Ba_7M^{3+}{}_6Al_2O_{19}$, in which the same oxygen-deficient blocks $Ba_2M^{3+}AlO_5$ (as for $Ba_5M_2Al_2ZrO_{13}$ [32]) are intergrown with a perovskite-like block $Ba_3M^{3+}{}_4O_9 \equiv Ba_3\square M^{3+}{}_4O_9\square_3$, containing barium and oxygen vacancies (□). The structures of all these compounds contain tetrahedra connected by their vertices and forming $[Al_2O_7]$-dimers, which alternate with octahedrally coordinated M^{3+}-cations [33]. For such structures, the process of incorporating OH-groups is realized without acceptor doping and is due to the presence of coordination-unsaturated Ba^{2+}-containing polyhedra in the hexagonal *h′*-layers. The degree of hydration is determined by the size of the interlayer space, which is sufficient to place the OH^--groups. Proton transport depends largely on the nature of the cation located in the octahedron and on the degree of ordering of the cations in the tetrahedra and octahedra.

Summarizing the scientific literature on proton transport in hexagonal perovskites, we can conclude that there is no general strategy for optimizing proton transport in such structures yet. The state of the issue is still at the stage of accumulation of the experimental material. In structural terms, such compounds are significantly more complex than classical perovskites ABO_3; therefore, establishing the «structure-defect structure-properties» correlation is a very difficult task.

We recently reported proton and oxide-ion conduction in the cation- and oxygen-deficient hexagonal perovskite $Ba_7In_6Al_2O_{19}$ [34]. However, acceptor doping has not been previously performed for this phase, and its effect on hydration and transport properties has not been studied. In this work, we prepared a new complex oxide in which some of the indium ions are replaced by zinc $Ba_7In_{5.9}Zn_{0.1}Al_2O_{18.95}$. We showed that with increasing lattice parameters and increasing number of oxygen vacancies the degree of hydration increased, and proton and oxide ion transport improved. Doping significantly increased the ionic transport numbers.

2. Experimental

The Zn^{2+}-doped phase $Ba_7In_{5.9}Zn_{0.1}Al_2O_{18.95}$ and the parent compound $Ba_7In_6Al_2O_{19}$ were prepared by a solid state technique according to the following reactions:

$$7\ BaCO_3 + Al_2O_3 + 3\ In_2O_3 \rightarrow Ba_7In_6Al_2O_{19} + 7\ CO_2 \tag{1}$$

$$\begin{gathered} 7\ BaCO_3 + Al_2O_3 + 2.95\ In_2O_3 + 0.10\ ZnO \rightarrow \\ \rightarrow Ba_7In_{5.9}Zn_{0.1}Al_2O_{18.95} + 7\ CO_2 \end{gathered} \tag{2}$$

The preliminary dried starting reagents $BaCO_3$ (99.9999% purity, REACHIM, Russia), In_2O_3 (99.99% purity, REACHIM, Russia), Al_2O_3 (99.99% purity, REACHIM, Russia), ZnO (99.99% purity, REACHIM, Russia) were weighed in stoichiometric quantities, then ground in an agate mortar with ethanol. The calcination of the powder mixtures was performed according to the following scheme: 800, 1000, 1100 °C (24 h at each stage), with intermediate grinding after each heating step. The ceramic samples were obtained by pressing powders in cylindrical pellet form and sintering at 1250 °C for 24 h. The relative densities, measured from the mass and dimensions of the sintered pellets, were ~95% of the theoretical X-ray density.

The phase purity was studied vai powder X-ray diffraction XRD on a Bruker Advance D8 diffractometer with Cu Kα radiation. The crystal structures of hydrated and dehydrated samples were checked by Rietveld refinement using FULLPROF software. For the XRD and TG investigations the dehydrated samples were prepared by heat treatment at 1100 °C for 3 h and then cooled in dry argon ($pH_2O = 3.5 \cdot 10^{-5}$ atm). The hydrated samples were obtained by slow cooling from 1100 to 150 °C (1 °C/min) under a flow of wet argon (99.999% purity, $pH_2O = 1.93 \cdot 10^{-2}$ atm).

TG investigations were carried out on a Simultaneous Thermal Analyzer STA 409 PC analyzer (Netzsch) coupled with a quadrupole mass spectrometer QMS 403 C Aëolos (Netzsch). The samples were heated at the rate of

10 °C/min in the temperature range of 40–1100 °C under a flow of Ar in a corundum crucible. For TG measurements the powder samples were hydrated as described above.

For electrical measurements both opposite surfaces of the tablet were coated with Pd-Ag paste electrodes, and then the electrodes were fired at 1000 °C for 3 h. The AC conductivity of the samples was measured by the 2-probe method using a Z-1000P impedance spectrometer (Elins, RF) within the frequency range of 1–10^6 Hz. The bulk resistances were calculated from the complex impedance plot using the Zview software fitting.

The conductivity measurements were performed at varying temperature under dry and wet air. The temperature dependencies were measured with a cooling rate of 10/min over the temperature range of 300–900 °C every 10–20 °C; at each temperature the sample was kept until the constant resistance values were attained. The «wet» atmosphere was obtained by bubbling the gas at room temperature first through distilled water and then through saturated solution of KBr ($pH_2O = 1.93 \cdot 10^{-2}$ atm). The «dry» atmosphere was produced by circulating the gas through P_2O_5 ($pH_2O = 3.5 \cdot 10^{-5}$ atm). The humidity of gases was monitored by an H_2O sensor («Honeywell» HIH-3610, USA).

The measurements of conductivities vs pO_2 were carried out in the temperature range of 500–800 °C by an electrochemical method using an electrochemical pump and an oxygen sensor (both based on yttrium-stabilized zirconium oxide), connected to the Zirconia-M automatic regulator [35]. The range of oxygen partial pressure was 10^{-18}–0.21 atm. The measurements were performed under dry and wet atmospheres. The «wet» atmosphere was obtained by circulating the gas at room temperature through saturated solution of KBr ($pH_2O = 1.93 \cdot 10^{-2}$ atm); the «dry» atmosphere was produced by circulating the gas through P_2O_5 ($pH_2O = 3.5 \cdot 10^{-5}$ atm).

3. Results and Discussions

3.1. X-ray phase analysis

Room temperature X-ray diffraction (XRD) results showed that the sample $Ba_7In_{5.9}Zn_{0.1}Al_2O_{18.95}$ was single phase and characterized by hexagonal symmetry (space group $P6_3/mmc$). Figures 1a and b present an example of profile fitting for the $Ba_7In_{5.9}Zn_{0.1}Al_2O_{18.95}$ sample and the crystal structure, respectively. The obtained lattice parameters and cell volumes are shown in Table 1. The cell parameters for the undoped $Ba_7In_6Al_2O_{19}$ phase were in good agreement with the previously reported data [34]. The substitution of In^{3+} ions by Zn^{2+} leads to an increase in the unit cell parameters and the unit cell volume (Table 1) despite the smaller radius of the dopant ($r_{In^{3+}}$ = 0.80 Å, $r_{Zn^{2+}}$ = 0.74 Å for a coordination number of 6) [36]. We believe that this is due to the appearance of charged defects, which lead to additional repulsion between the layers. It should be said that similar effects were observed for doped phases with the Ruddlesden-Popper structure. For example, the introduction of a dopant with a smaller ionic radius with respect to the host atoms causes lattice expansion, which was previously described for RP structures [37–39].

The incorporation of water was accompanied by an increase in the lattice parameters (more significant for the *c* parameters) and, accordingly, an increase in the cell volumes (Table 1). This behavior is typical for layered structures, which indicates the predominant location of the OH^--groups in the interlayer space, that is, in the oxygen-deficient *h*′-layer in our case (this corresponds to a more significant increase in the c parameter). Hydrolytic decomposition of the phases did not occur; no impurity phases were detected.

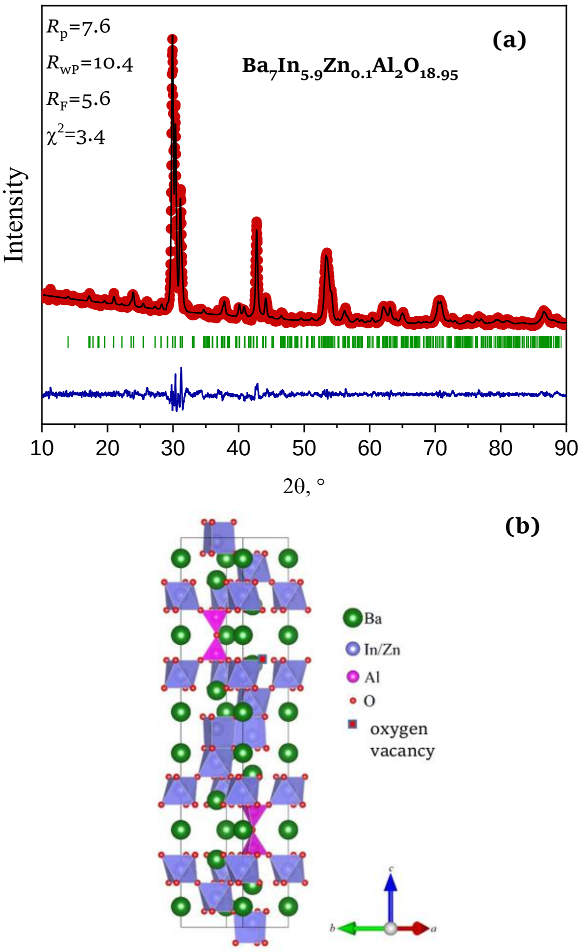

Figure 1 Rietveld profile fitting of powder X-ray diffraction pattern for the dehydrated $Ba_7In_{5.9}Zn_{0.1}Al_2O_{18.95}$ sample. The experimental data are given as red circles, the fitted profile as solid black line. The vertical bars indicate the expected positions of the Bragg peaks upon refinement in the space group $P6_3/mmc$. The bottom blue line represents the difference between the calculated and experimental data (a). Crystal structures of the investigated sample (b).

Table 1 Unit cell parameters and cell volumes for dehydrated $Ba_7In_6Al_2O_{19}$, $Ba_7In_{5.9}Zn_{0.1}Al_2O_{18.95}$ samples and hydrated $Ba_7In_6Al_2O_{19} \cdot 0.41H_2O$, $Ba_7In_{5.9}Zn_{0.1}Al_2O_{18.95} \cdot 1.42H_2O$ samples.

Phase	a, Å	c, Å	*V*, Å³
$Ba_7In_6Al_2O_{19}$	5.921(2)	37.717(4)	1145.2(3)
$Ba_7In_{5.9}Zn_{0.1}Al_2O_{18.95}$	5.968(9)	38.055(4)	1174.1(8)
$Ba_7In_6Al_2O_{19} \cdot 0.41H_2O$	5.925(7)	37.721(2)	1147.5(4)
$Ba_7In_{5.9}Zn_{0.1}Al_2O_{18.95} \cdot 1.42H_2O$	5.970(3)	38.079(5)	1175.5(5)

DOI: 10.15826/chimtech.2024.11.4.03

3.2. Hydration processes

The possibility of water uptake can be established by TG measurements coupled with mass spectrometry (MS) analysis. Figure 2 shows TG and MS(H_2O)-curves for the preliminarily hydrated $Ba_7In_{5.9}Zn_{0.1}Al_2O_{18.95}$ sample in comparison with the TG curve of the undoped phase. The main mass loss occurs in the temperature range of 150–500 °C, which is accompanied by two MS(H_2O) effects. In addition, at a high temperature ~750 °C there is also a slight loss of mass due to the release of water, which is the third effect on the MS(H_2O) curve. Mass stabilization occurs above 900 °C. Thus, the Zn^{2+}-doped sample is capable of hydration, and the degree of hydration was 1.42 mol H_2O which is significantly greater than that of the undoped phase (0.41 mol H_2O).

The formation of proton defects for phases with unoccupied crystallographic oxygen positions can be described by the following quasi-chemical reactions in the Kröger-Vink notation:

$$V_O^X + O_O^X + H_2O \leftrightarrow OH_O^{\bullet} + OH'_{V_O^x}, \qquad (3)$$

where V_O^X is the structural oxygen vacancy, O_O^X is the oxygen atom in a regular position, $OH_O^{\bullet}$ is the hydroxyl group in the oxygen sublattice, $OH'_{V_O^x}$ is the hydroxyl group in the position of the structural oxygen vacancy.

On the other hand, the oxygen vacancies that appear during acceptor doping $V_O^{\bullet\bullet}$ are also capable of incorporating protons (OH-groups):

$$H_2O + V_O^{\bullet\bullet} + O_O^X \rightleftarrows 2(OH)_O^{\bullet}, \qquad (4)$$

where $V_O^{\bullet\bullet}$ – oxygen vacancy, $OH_O^{\bullet}$ – hydroxyl group in the oxygen sublattice. These equations demonstrate the correlation between the concentration of oxygen vacancies and the degree of hydration (i.e., the concentration of protons).

However, the effect of increasing the degree of hydration is not due to additional oxygen deficiency as a result of doping, since it is more significant than the resulting concentration of oxygen vacancies. That is, the appearance of oxygen vacancies [$V_O^{\bullet\bullet}$] = 0.05 upon doping does not correspond to such significant increase in the concentration of protons (increase by 1 mole of water). As it is known, the ability of phases with a block (layered) structure to hydrate occurs without acceptor doping and is due to the introduction of OH^--groups into the interlayer space [23]. Accordingly, the solubility limit for such phases does not correlate with the concentration of oxygen vacancies, but is determined by the sufficient space to place OH^--groups. Thus, the solubility limit is determined by changing the geometric factor, that is, increasing the cell parameters in our case. As mentioned earlier [34], the capability of the compound $Ba_7In_6Al_2O_{19}$ to incorporate water is due to the presence of oxygen-deficient hexagonal layers, where barium is bonded in a 9-coordinate geometry (i.e. with nine oxygen atoms) [40]. Accordingly, such coordinatively unsaturated barium polyhedron can incorporate OH^--groups and increase its coordination number. Thus, sufficient space in the hexagonal layers is necessary for the arrangement of OH^- groups. Consequently, an increase in the cell volume during doping facilitates an increase in water uptake. Therefore, the strategy of increasing the cell volume and, as a consequence, the size of the interlayer space is successful for increasing the proton concentration in compounds with hexagonal structures. Such features of the hydration character of block (layered) phases distinguish them from classical doped perovskites, for which a correlation between the concentration of oxygen vacancies and the concentration of protons is observed.

3.3. Electrical conductivity

3.3.1. Dry conditions

In Figure 3 the evolution of the impedance spectra of $Ba_7In_{5.9}Zn_{0.1}Al_2O_{18.95}$ sample is shown as a Nyquist plot for several temperatures. This view of the spectra was typical of the investigated compounds under different experimental conditions. As can be seen, three semicircles in the complex *Z′-Z″* plane, corresponding to the bulk, grain-boundary and electrode components were observed. The main contribution is represented by the grain boundary process; these semicircles have capacitances of ~10^{-10}–10^{-9} F·cm⁻¹. The capacitance for the first semicircle, starting from the «0»-coordinates and representing the bulk response, is determined to be ~10^{-11} F·cm⁻¹; the capacitance for the third low-frequency semicircle, representing the electrode response, is ~10^{-7}–10^{-6} F·cm⁻¹.

The calculated bulk, grain-boundary and total conductivities of $Ba_7In_{5.9}Zn_{0.1}Al_2O_{18.95}$ as a function of temperature are shown in Figure 4. The grain boundary conductivity is more than one order of magnitude lower than the bulk conductivity, and the total conductivity is determined by the grain boundary conductivity (for both dry and wet air).

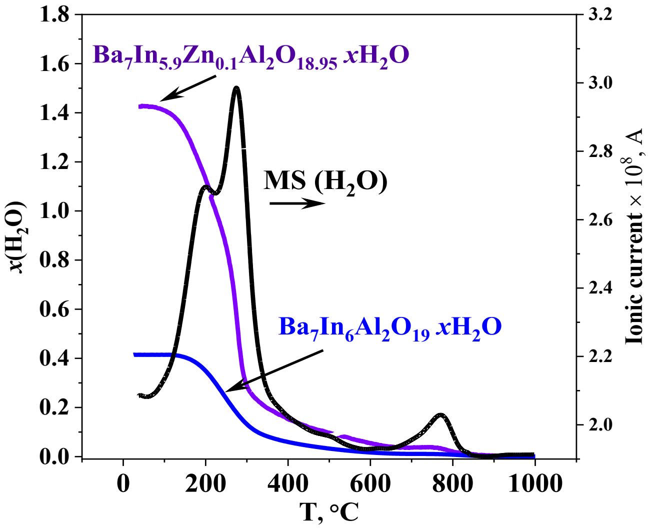

Figure 2 TG and MS(H_2O) curves for $Ba_7In_{5.9}Zn_{0.1}Al_2O_{18.95}$, and the TG curve for $Ba_7In_6Al_2O_{19}$.

There are little data in the literature concerning the analysis of hodographs for hexagonal perovskites and the extraction of different contributions, and most of the data show only conductivity dependences. However, a number of articles have shown that for such structures a more significant contribution of grain boundaries is observed [25, 41, 42]. The general explanation is that the state of the grain boundaries differs from the bulk, but an analysis of the reasons requires separate studies.

The electrode response observed in the low-frequency region is represented by a very small semicircle (that is, low polarization resistance), which indicates the reversibility of the electrodes.

A comparison of the conductivities of the doped and undoped samples is shown in Figure 5. The conductivity of the Zn^{2+}-doped phase is higher than that of the pure phase over the entire studied temperature range, which is presumably due to the formation of oxide-ion vacancies as a result of the replacement of In^{3+} with Zn^{2+}. The differences reached half an order of magnitude. To separate the total conductivity into partial contributions, the conductivity was measured vs the partial oxygen pressure.

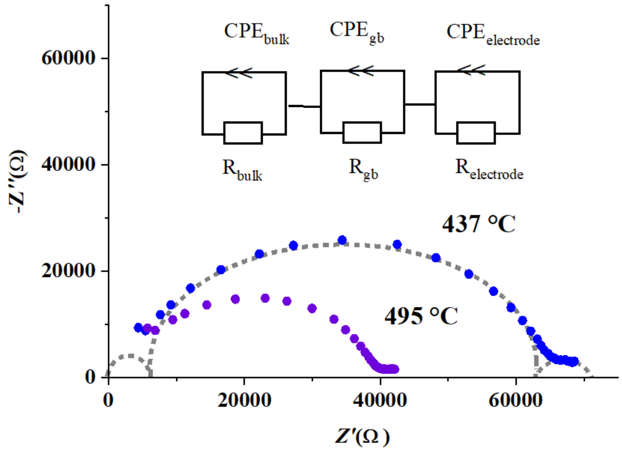

Figure 3 Impedance spectra of $Ba_7In_{5.9}Zn_{0.1}Al_2O_{18.95}$ at different temperatures in dry air (pH_2O = 3.5·10^{-5} atm).

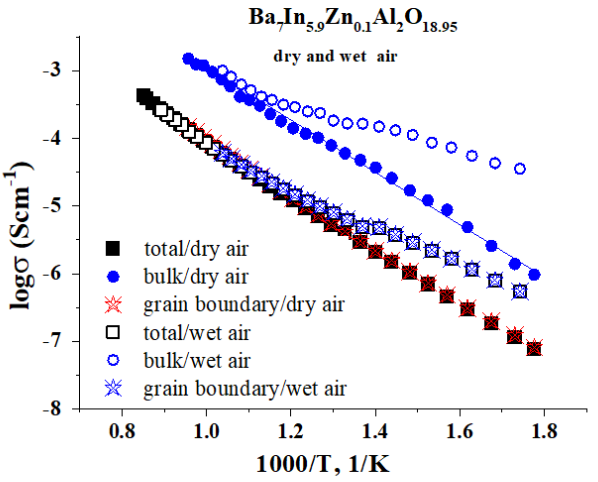

Figure 4 Temperature dependencies of the bulk, grain-boundary and total conductivities for $Ba_7In_{5.9}Zn_{0.1}Al_2O_{18.95}$ in dry (pH_2O = 3.5·10^{-5} atm, filled signs) and wet (pH_2O = 1.93·10^{-2} atm, open signs) air.

Figure 6 shows a comparison of the dependencies of the conductivities vs the oxygen partial pressure at different temperatures for dry conditions (pH_2O = 3.5·10^{-5} atm) for the samples $Ba_7In_{5.9}Zn_{0.1}Al_2O_{18.95}$ and $Ba_7In_6Al_2O_{19}$. Both samples exhibited a plateau region in the range of oxygen partial pressures $10^{-18} \le pO_2 \le 10^4$ atm. The independence of conductivity from pO_2 indicates the dominant ionic nature of conductivity; taking into account the specificity of disordering, namely, the presence of oxygen deficiency, it can be concluded that the nature of ionic conductivity is oxide-ionic. As can be seen, the ionic conductivity of Zn^{2+}-doped phase is higher than that of the parent phase.

Under oxidizing conditions ($pO_2 > 10^{-4}$ atm) the conductivity increased with increasing pO_2, which indicates the appearance of a contribution of hole conductivity. The formation of holes can be described by the following quasi-chemical equation:

$$V_O^X + \frac{1}{2}O_2 \leftrightarrow 2h^{\bullet} + O''_{V_O^X} \qquad (5)$$

where V_O^X is the structural oxygen vacancy, $O''_{V_O^X}$ is the oxygen atom in the position of the structural oxygen vacancy, $h^{\bullet}$ is the hole.

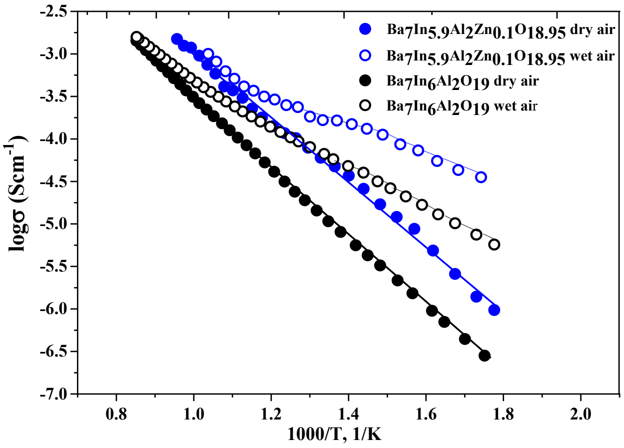

Figure 5 Comparison of the temperature dependencies of the conductivities of doped $Ba_7In_{5.9}Zn_{0.1}Al_2O_{18.95}$ and undoped $Ba_7In_6Al_2O_{19}$ samples in dry (pH_2O = 3.5·10^{-5} atm, filled signs) and wet (pH_2O = 1.93·10^{-2} atm, open signs) air.

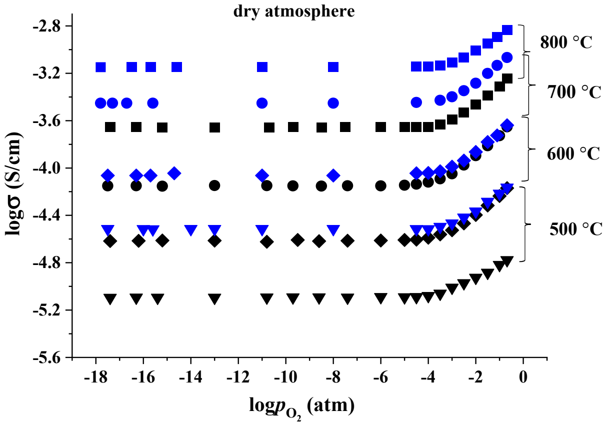

Figure 6 Dependencies of the conductivity vs oxygen partial pressure at different temperatures for $Ba_7In_{5.9}Zn_{0.1}Al_2O_{18.95}$ (blue symbols) and $Ba_7In_6Al_2O_{19}$ (black symbols) in a dry atmosphere.

The ionic transport numbers, calculated as $t_{O^{2-}} = \sigma_{O^{2-}}/\sigma_{tot}$ ($\sigma_{O^{2-}}$ – conductivity in the plateau region, σ_{tot} – total conductivity in air pO_2 = 0.21 atm) are shown in Table 2. The $Ba_7In_{5.9}Zn_{0.1}Al_2O_{18.95}$ sample exhibited mixed conductivity in air, and the oxygen-ionic transport numbers increased slightly with increasing temperature.

The temperature dependences of the oxide-ion conductivity of the doped phase and the parent phase are shown in Figure 7. The oxide-ion conductivity of the doped phase is higher by approximately 0.5 orders of magnitude over the studied temperature range. This can be explained, on the one hand, by an increase in the disordering of the oxygen sublattice, and on the other hand, by an increase in the lattice parameters, since an increase in the lattice parameters leads to a decrease in the metal-oxygen bond energy and facilitates ion transport. The activation energy of the oxide-ion conductivity was 0.89 eV, which is typical of the oxygen transport, and this value was close to the activation energy of the undoped phase.

3.3.2. Wet conditions

As seen from the temperature dependences of the conductivities (Figure 5), an increase in humidity is accompanied by a significant increase in conductivity (up to 1.5 orders of magnitude at 300 °C) and a decrease in the activation energy. This indicates the appearance of a proton contribution to the conductivity. According to thermogravimetry measurements (Figure 2), the intense change in mass as a result of the intercalation of water molecules into the crystal lattice occurs at temperatures below 600 °C. So, the increase in conductivity in a wet atmosphere compared with dry air and the decrease in activation energy at temperatures below 600 °C are due to the contribution of proton conductivity. At higher temperatures, the conductivities in dry and wet atmospheres are almost identical, which, according to TG data, corresponds to a sharp decrease in the proton concentration; accordingly, the contribution of proton conductivity decreases. The magnitude of the proton conductivity and its activation energy are discussed below.

The conductivity in wet air is also 0.75 orders of magnitude greater than that of the parent phase at 300 °C.

Figures 8, 9 show the results of the conductivity measurements under wet conditions as a function of the oxygen partial pressure for the Zn^{2+}-doped sample in comparison with the dry conditions and in comparison with the undoped phase $Ba_7In_6Al_2O_{19}$, respectively. In the region of oxygen partial pressures $10^{-18} \leq pO_2 \leq 10^{-2}$ atm, a plateau of conductivity independence is observed. This indicates the dominant ionic conductivity. In the region of $pO_2 > 10^{-2}$ atm, the conductivity increases slightly with increasing pO_2, as a result of the insignificant contribution of hole conductivity, and at a temperature of 500 °C the conductivity is practically independent of pO_2 in the entire studied range of partial oxygen pressures, which indicates dominant ionic transport.

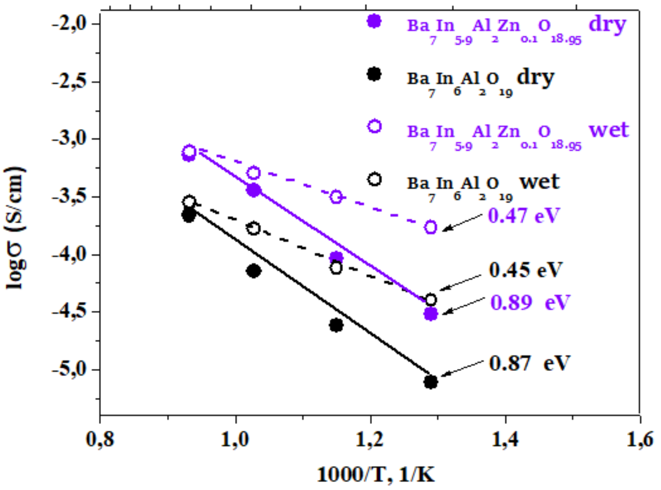

Figure 7 Temperature dependencies of the ionic conductivities of $Ba_7In_{5.9}Zn_{0.1}Al_2O_{18.95}$ in comparison with $Ba_7In_6Al_2O_{19}$ for dry (pH_2O = 3.5·10⁻⁵ atm, filled signs) and wet (pH_2O = 1.93·10⁻² atm, open signs) atmospheres.

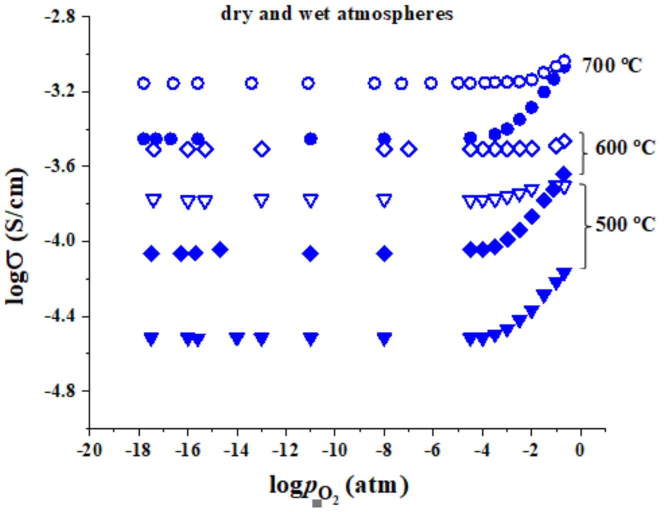

Figure 8 Dependencies of the conductivity vs oxygen partial pressure at different temperatures for $Ba_7In_{5.9}Zn_{0.1}Al_2O_{18.95}$ in dry (filled signs) and wet (open signs) atmospheres.

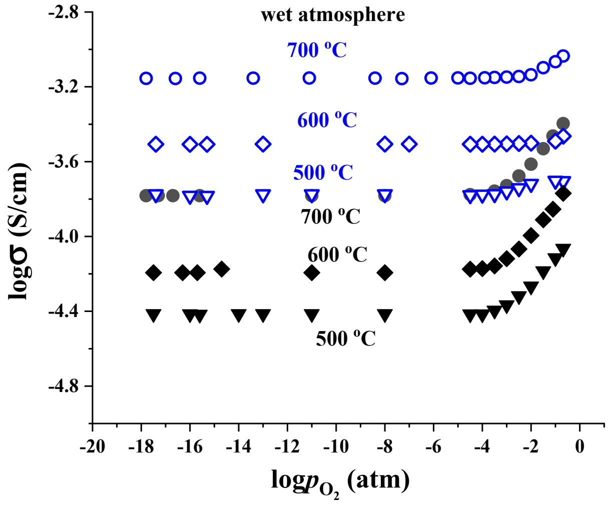

Figure 9 Dependencies of the conductivity vs oxygen partial pressure at different temperatures for $Ba_7In_{5.9}Zn_{0.1}Al_2O_{18.95}$ (blue signs) in comparison with $Ba_7In_6Al_2O_{19}$ (black signs) in a wet atmosphere.

A comparison of the conductivity isotherms of both the doped and undoped samples (Figure 9) revealed that the doped sample exhibited higher values of conductivity over the entire investigated pO_2 region.

The partial oxide-ion and proton conductivities were determined using data on conductivity as a function of oxygen partial pressure at different humidities. The calculations were made based on modeling in accordance with defect formation reactions, which were previously shown in the works [43–45].

In general, the conductivity in the plateau region is represented as a sum $\sigma = \sigma_{O^{2-}} + \sigma_{H^+}$. However, since the oxide-ion conductivity is significantly less than the proton conductivity, $\sigma_{O^{2-}} \ll \sigma_{H^+}$, at temperatures below 600 °C, the total conductivity is essentially the proton conductivity $\sigma \sim \sigma_{H^+}$. A comparison of the temperature dependences of the proton conductivities for the doped and parent phases is presented in Figure 7. In a wet atmosphere the conductivity of the doped phase is higher, and the difference reaches 0.75 orders of magnitude at 500 °C. That is, doping led to an increase in the proton conductivity. This is due to an increase in proton concentration according to the TG data. The proton conductivity is characterized by an activation energy of 0.47 eV, which is typical for proton conduction. The proton transport numbers calculated as $t_{H^+} = \sigma_{H^+}/\sigma_{tot}$ (air pO_2 = 0.21 atm, wet conditions) are presented in Table 2 confirm the abovementioned relationships.

Thus, the strategy of introducing zinc into the indium sublattice in hexagonal perovskite $Ba_7In_6Al_2O_{19}$ is promising in terms of both increasing the proton concentration and increasing the oxide-ion and proton conductivities.

A comparison of the temperature dependences of conductivity in wet air for the Zn^{2+}-doped sample $Ba_7In_{5.9}Zn_{0.1}Al_2O_{18.95}$ with other phases with a block (layered) structure is shown in Figure 10. The conductivity of the studied phase was lower than the conductivity of the best proton conductors with a hexagonal structure. However, at the same time, these conductivity values are typical of many phases and are within the limits of acceptable conductivity values for the proton-conducting electrolytes. Since for such structures variation in composition can significantly affect proton conductivity, it is obvious that to optimize the proton conductivity it is possible to search for other compositions based on $Ba_7In_6Al_2O_{19}$ or to use the co-doping method.

4. Limitations

One of the limitations is the interpretation of the data on the significant increase in lattice parameters upon doping. At present, the difficulties are due to the complexity of the structural analysis, since this is a very complex structure and it is difficult to assign coordinates to the dopant, which will be done in the future when wider dopant concentrations will have been studied.

Table 2 Oxide-ion transport numbers (dry air, $pH_2O = 3.5\cdot10^{-5}$ atm) and proton transport numbers (wet air, $pH_2O = 1.93\cdot10^{-2}$ atm) for $Ba_7In_{5.9}Zn_{0.1}Al_2O_{18.95}$ (%).

Temperature, °C	500	600	700	800
$t_{O^{2-}}$	38	39	40	46
t_{H^+}	97	91	78	–

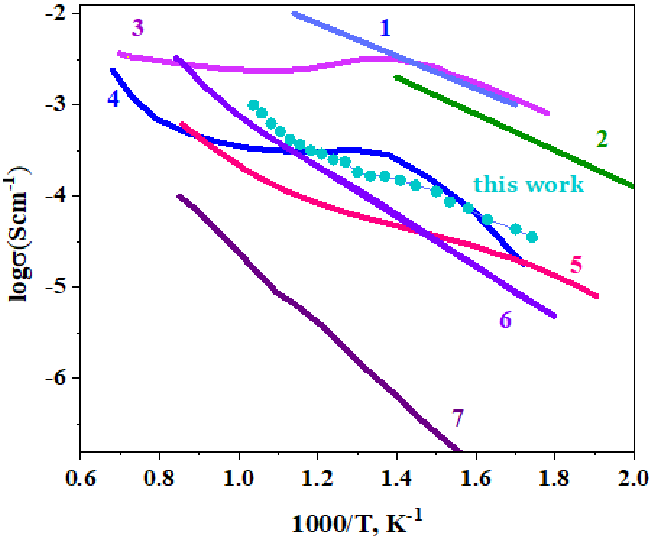

Figure 10 Comparison of the temperature dependencies of the conductivities in wet air for $Ba_7Nb_{3.8}Mo_{1.2}O_{20.1}$ (1) [46], $Ba_7Nb_4MoO_{20}$ (2) [20], $Ba_5Er_2Al_2ZrO_{13}$ (3) [24], $Ba_5Lu_2Al_2ZrO_{13}$ (4) [24], $Ba_5In_2Al_2ZrO_{13}$ (5) [34], $BaLaIn_{0.5}Y_{0.5}O_4$ (6) [47], $BaLaInO_4$ (7) [47] and $Ba_7In_{5.9}Zn_{0.1}Al_2O_{18.95}$ (this work, circles).

5. Conclusions

In the present study the influence of the introduction of zinc into the indium sublattice of the hexagonal perovskite $Ba_7In_6Al_2O_{19}$ on hydration and conductivity was investigated.

The hexagonal perovskite $Ba_7In_{5.9}Zn_{0.1}Al_2O_{18.95}$ was synthesized by the solid-state method for the first time. The investigated phase had a hexagonal structure with a space group of P6$_3$/mmc. The substitution of In^{3+} by Zn^{2+} led to an increase in the lattice parameters. The lattice parameters for $Ba_7In_{5.9}Zn_{0.1}Al_2O_{18.95}$ were a = 5.968(9) Å, c = 38.055(4) Å vs a = 5.921(2) Å, c = 37.717(4) Å for $Ba_7In_6Al_2O_{19}$.

The studied sample $Ba_7In_{5.9}Zn_{0.1}Al_2O_{18.95}$ was capable of water incorporation and, in comparison with the undoped phase, a significant increase in the degree of hydration was observed (1.42 mol H_2O for $Ba_7In_{5.9}Zn_{0.1}Al_2O_{18.95}$ *vs* 0.41 mol H_2O for $Ba_7In_6Al_2O_{19}$). This is due to an increase in the cell volume and, as a consequence, an increase in the size of the oxygen-deficient hexagonal h′-blocks.

The electrical conductivity was investigated by the electrochemical impedance technique by varying T, pO_2 and pH_2O. It was found that Zn^{2+} doping led to an increase in oxygen-ion (dry conditions) and proton (wet conditions) conductivities due to increase in the concentration of oxygen vacancies and protons, respectively.

• Supplementary materials

No supplementary materials are available.

DOI: 10.15826/chimtech.2024.11.4.03

• Funding

This work was supported by the Russian Science Foundation and Government of the Sverdlovsk region (grant № 24-13-20026), https://rscf.ru/project/24-13-20026/.

RSF | Russian Science Foundation

• Acknowledgments

None.

• Author contributions

Conceptualization: I.E.A.
Methodology: I.E.A., D.V.K.
X-ray diffraction analysis: R.D.A.
TG measurements: D.V.K.
Conductivity measurements: A.V.B., S.S.N.
Writing – original draft: I.E.A.
Writing – review & editing: I.E.A., D.V.K.

• Conflict of interest

The authors declare no conflict of interest.

• Additional information

Author IDs:
Animitsa Irina, Scopus ID 6603520951;
Daniil Korona, 13406057200;
Arina Bushueva, 59307369500;
Roman Andreev, 57737857400;
Sergey Nokhrin, 56634307800.

Website:
Ural Federal University, https://urfu.ru/en/.

References

1. Takahashi T, Iwahara H. Solid state ionics: proton conduction in perovskite type solid solutions. Rev Chim Miner. 1980;17(4):243–253. doi:10.1002/chin.198114014
2. Iwahara H, Esaka T, Uchida H, Maeda N. Proton conduction in sintered oxides and its application to steam electrolysis for hydrogen production. Solid State Ionics. 1981;3–4:359–363. doi:10.1016/0167-2738(81)90113-2
3. Karuppiah K, Ashok A. Review on Proton and Oxide Ion Conducting Perovskite Materials for SOFC Applications. Nanomater Energy. 2019;8(1):1–8. doi:10.1680/jnaen.18.00004
4. Medvedev D, Murashkina A, Pikalova E, Demin A, Podias A, Tsiakaras P. BaCeO$_3$: Materials development, properties and application. Prog Mater Sci. 2014;60:72–129. doi:10.1016/j.pmatsci.2013.08.001
5. Tayyab M, Rauf S, Khan AZ, Tayyab Z, Khan K, Hussain I, Hussain MB, Waseem M, Alodhayb AN, Fu XZ, Qasim M, Tian Y. Breaking barriers: Novel approaches to proton-conducting oxide materials. Ceram Int. 2024. doi:10.1016/j.ceramint.2024.06.008
6. Scholten MJ, Schoonman J, van Miltenburg JC, Oonk HAJ. Synthesis of strontium and barium cerate and their reaction with carbon dioxide. Solid State Ionics. 1993;61:83–91. doi:10.1016/0167-2738(93)90338-4
7. Ma G, Shimura T, Iwahara H. Ionic conduction and nonstoichiometry in Ba$_x$Ce$_{0.90}$Y$_{0.10}$ O$_{3-\alpha}$. Solid State Ionics. 1998;110:103–110. doi:10.1016/S0167-2738(98)00130-1
8. Ryu KH, Haile SM. Chemical stability and proton conductivity of doped BaCeO$_3$ –BaZrO$_3$ solid solutions. Solid State Ionics. 1999;125:355–367. doi:10.1016/S0167-2738(99)00196-4
9. Radojkovic A, Zunic M, Savic SM, Brankovic G, Brankovic Z. Chemical stability and electrical properties of Nb doped BaCe$_{0.9}$Y$_{0.1}$O$_{3-\delta}$ as a high temperature proton conducting electrolyte for IT-SOFC. Ceram Int. 2013;39(1):307–313. doi:10.1016/j.ceramint.2012.06.026
10. Kannan R, Singh K, Gill S, Furstenhaupt T, Thangadurai V. Chemically Stable Proton Conducting Doped BaCeO$_3$ -No More Fear to SOFC Wastes. Sci Rep. 2013;3:1–5. doi:10.1038/srep02138
11. Medvedev DA, Lyagaeva JG, Gorbova EV, Demin AK, Tsiakaras P. Advanced materials for SOFC application: Strategies for the development of highly conductive and stable solid oxide proton electrolytes. Prog Mater Sci. 2016;75:38–79. doi:10.1016/j.pmatsci.2015.08.001
12. Medvedev D, Lyagaeva J. Plaksin S, Demin A, Tsiakaras P. Sulfur and carbon tolerance of BaCeO$_3$-BaZrO$_3$ proton-conducting materials. J Power Sources. 2015;273:716–723. doi:10.1016/j.jpowsour.2014.09.116
13. Sazinas R, Bernuy-Lopez C, Einarsrud M-A. Grande T. Effect of CO$_2$ exposure on the chemical stability and mechanical properties of BaZrO$_3$-ceramics. J Am Ceram Soc. 2016;99:3685–3695. doi:10.1111/jace.14395
14. Lacz A, Silarska K, Piecha I, Pasierb P. Structure, chemical stability and electrical properties of BaCe$_{0.9}$Y$_{0.1}$O$_{3-\delta}$ proton conductors impregnated with Ba$_3$(PO$_4$)$_2$. Int J Hydrog Energy. 2016;41:13726–13735. doi:10.1016/j.ijhydene.2016.06.009
15. Somekawa T, Matsuzaki Y, Sugahara M, Tachikawa Y, Matsumoto H, Taniguchi S, Sasaki K. Physicochemical properties of Ba(Zr,Ce)O$_{3-\delta}$-based proton-conducting electrolytes for solid oxide fuel cells in terms of chemical stability and electrochemical performance. Int J Hydrog Energy. 2017;42(26):16722–16730. doi:10.1016/j.ijhydene.2017.04.26
16. Stavrakakis E, West M, Johnston S, McIllwaine R, Poulidi D. Hydration, CO2 stability and wireless electrochemical promotion studies on yttria-doped Ba(Ce,Zr)O$_3$ perovskites. Ionics. 2019;25:1243–1257. doi:10.1007/s11581-019-02836-6
17. Guo H, Li Y, Jiang L, Sha Y, Guoa S, Han D. Transport properties of the Ba(Zr,Ce,Y,Yb)O$_{3-\delta}$ proton conductor: the real role of co-substitution of Y and Yb. J Mater Chem A. 2024;12:5875–5884. doi:10.1039/D3TA07486B
18. Saito K, Umeda K, Fujii K, Mori K, Yashima M. High Proton Conduction by Full Hydration in Highly Oxygen Deficient Perovskite. J Mater Chem A. 2024;12(22):13310–13319. doi:10.1039/D4TA01978D
19. Yang X, Fernandez-Carrión AJ, Geng X, Kuang X. B-Site Deficient Hexagonal Perovskites: Structural Stability, Ionic Order-Disorder and Electrical Properties. Prog Solid State Chem. 2024;74:1-19. doi:10.1016/j.progsolidstchem.2024.100459
20. Fop S, McCombie KS, Wildman EJ, Skakle JMS, Irvine JTS, Connor PA, et al. High oxide ion and proton conductivity in a disordered hexagonal perovskite. Nat Mater. 2020;19:752–775. doi:10.1038/s41563-020-0629-4
21. Fop S, McCombie KS, Wildman EJ, Skakle JMS, McLaughlin AC. Hexagonal perovskite derivatives: a new direction in the design of oxide ion conducting materials. Chem Commun. 2019;55:2127–2137. doi:10.1039/C8CC09534E
22. Fop S. Solid oxide proton conductors beyond perovskites. J Mater Chem A. 2021;9:18836–18856. doi:10.1039/d1ta03499e
23. Tarasova NA, Animitsa IE, Galisheva AO, Medvedev DA. Layered and Hexagonal Perovskites as Novel Classes of Proton-

Conducting Solid Electrolytes. A Focus Review. Electrochem Mater Technol. 2022;1:20221004. doi:10.15826/elmattech.2022.1.004

24. Murakami T, Hester J, Yashima M. High Proton Conductivity in $Ba_5Er_2Al_2ZrO_{13}$, a Hexagonal Perovskite-Related Oxide with Intrinsically Oxygen-Deficient Layers. J Am Chem Soc. 2020;142:11653–11657. doi:10.1021/jacs.0c02403
25. Matsuzaki K, Saito K, Ikeda Y, Nambu Y, Yashima M. High Proton Conduction in the Octahedral Layers of Fully Hydrated Hexagonal Perovskite-Related Oxides. J Am Chem Soc. 2024;146:18544–18555. doi:10.1021/jacs.4c04325
26. Andreev R, Korona D, Anokhina I, Animitsa I. Proton and oxygen-ion conductivities of hexagonal perovskite $Ba_5In_2Al_2ZrO_{13}$. Mater. 2022;15(11):1–18. doi:10.3390/ma15113944
27. Andreev RD, Korona DV, Anokhina IA, Gilev AR, Animitsa IE. Transport properties of In^{3+}-and Y^{3+}-doped hexagonal perovskite $Ba_5In_2Al_2ZrO_{13}$. Russ J Electrochem. 2023;(59):190–203. doi:10.1134/S1023193523030035
28. Andreev RD, Animitsa IE Protonic transport in the novel complex oxide $Ba_5Y_{0.5}In_{1.5}Al_2ZrO_{13}$. Ionics. 2023;29(11):4647–4658. doi:10.1007/s11581-023-05187-5
29. Andreev RD, Korona DV, Vlasov MI, Animitsa IE. Protonic ceramics $Ba_5In_{2-x}Y_xAl_2ZrO_{13}$ with the perovskite-related hexagonal structure for solid oxide fuel cells: synthesis, optical band gap and transport properties. Ceram Int. 2024. doi:10.1016/j.ceramint.2024.04.227
30. Suzuki Y, Murakami T, Fujii K, Hester JR, Yasui Y, Yashima M. Simultaneous reduction of proton conductivity and enhancementof oxide-ion conductivity by aliovalent doping in $Ba_7Nb_4MoO_{20}$. Inorg Chem 2022;61:7537–7545. doi:10.1021/acs.inorgchem.2c00671
31. Sakuda Y, Hester JR, Yashima M. Improved oxide-ion and lower proton conduction of hexagonal perovskite-related oxides based on $Ba_7Nb_4MoO_{20}$ by Cr^{6+} doping. J Ceram Soc Jpn. 2022;130:442–447. doi:10.2109/jcersj2.21192
32. Shpanchenko RV, Abakumov AM, Antipov EV, Nistor, Tendeloo G, Amelinckx SJ. Structural study of the new complex oxides $Ba_{5-y}Sr_yR_{2-x}Al_2Zr_{1+x}O_{13+x/2}$ (R = Gd-Lu, Y, Sc). Solid State Chem. 1995;118:180–192. doi:10.1006/jssc.1995.1329
33. Shpanchenko RV, Nistor L, Tendeloo G, Amelinckx S, Antipov EV, Kovba LM. High–resolution electron microscopic study of $Ba_7Sc_6Al_2O_{19}$ and related phases. J Solid State Chem. 1994;113:193–204. doi:10.1006/jssc.1994.1359
34. Andreev R, Animitsa I. Transport properties of intergrowth structures $Ba_5In_2Al_2ZrO_{13}$ and $Ba_7In_6Al_2O_{19}$. Appl Sci. 2023;13(6):1–14. doi:10.3390/app13063978
35. Zirconia Project. Available online: https://zirconiaproject.wordpress.com/devices/zirconiam/
36. Shannon RD. Revised effective ionic radii and systematic studies of interatomic distances in halides and chalcogenides. Acta Cryst. 1976; A32:751–767. doi:10.1107/S0567739476001551
37. Tarasova N, Animitsa I, Galisheva A, Korona D. Incorporation and Conduction of Protons in Ca, Sr, Ba-Doped $BaLaInO_4$ with Ruddlesden-Popper Structure. Mater. 2019;12(10):1–14. doi:10.3390/ma12101668
38. Troncoso L, Alonso JA, Fernández-Díaz MT, Aguadero A. Introduction of interstitial oxygen atoms in the layered perovskite $LaSrIn_{1-x}B_xO_{4+\delta}$ system (B=Zr, Ti). Solid State Ionics. 2015;282:82–87. doi:10.1016/j.ssi.2015.09.014
39. Aguadero A, Alonso JA, Martínez-Lope MJ, Fernández-Díaz MT, Escudero MJ, Daza L. In situ high temperature neutron powder diffraction study of oxygen-rich $La_2NiO_{4+\delta}$ in air: correlation with the electrical behaviour. J Mater Chem. 2006;16:3402–3408. doi:10.1039/b605886h
40. Shpanchenko RV, Antipov EV, Paromova MV, Kovba LM. Crystal structure of $Ba_7Sc_6Al_2O_{19}$. Zhurnal Neorganicheskoi Khimii. 1991;136:1402–1407.
41. Unti LF Kultz, Grzebielucka EC, Chinelatto ASA, MatherGC, Chinelatto AL. Synthesis and electrical characterization of Ba_5Nb_4O15 and $Ba_5Nb_{3.9}M_{0.1}O_{(15-\delta)}$ (M = Ti, Zr) hexagonal perovskites. Ceram Int. 2019;45;5087–5092. doi:10.1016/j.ceramint.2018.11.211
42. McCombie KS, Wildman EJ, Fop S, Smith RI,. Skakle JMS, Mclaughlin AC. The Crystal Structure and Electrical Properties of the Oxide Ion Conductor $Ba_3WNbO_{8.5}$. J Mater Chem A. 2018;6;5290–5295. doi:10.1039/C7TA08989A
43. Frade JR. Theoretical behavior of concentration cells based on ABO_3 perovskite materials with protonic and oxygen-ion conduction. Solid State Ionics. 1995;78:87–97. doi:10.1016/0167-2738(95)00008-T
44. Baek HD. Modeling of electrical conductivity in high-temperature proton-conducting oxides. Solid State Ionics. 1998;110:255–262. doi:10.1016/S0167-2738(98)00138-6
45. Glöckner R, Neiman A, Larring Y, Norby T. Protons in $Sr_3(Sr_{1+x}Nb_{2-x})O_{9-3x/2}$ perovskite. Solid State Ionics. 1999;125:369–376. doi:10.1016/S0167-2738(99)00197-6
46. Sakuda Y, Murakami T, Avdeev M, Fujii K, Yasui Y, Hester JR, et al. Dimer-mediated cooperative mechanism of ultrafast-ion conduction in hexagonal perovskite-related oxides. Chem Mater. 2023;35:9774–9788. doi:10.1021/acs.chemmater.3c02378
47. Tarasova N, Galisheva A, Animitsa I, Korona D, Davletbaev K. Novel proton-conducting layered perovskite based on $BaLaInO_4$ with two different cations in B-sublattice: Synthesis, hydration, ionic (O^{2-}, H^+) conductivity. Int J Hydrog Energy. 2022;47:18972–18982. doi:10.1016/j.ijhydene.2022.04.112